Nanoscale subsurface imaging of nanocomposites via resonant difference-frequency atomic force ultrasonic microscopy

Sean A. Cantrell, John H. Cantrell, and Peter T. Lillehei
NASA Langley Research Center, Research and Technology Directorate, Hampton, Virginia 23681

Abstract:

A scanning probe microscope methodology, called resonant difference-frequency atomic force ultrasonic microscopy (RDF-AFUM), has been developed. The method employs an ultrasonic wave launched from the bottom of a sample while the cantilever of an atomic force microscope engages the sample top surface. The cantilever is driven at a frequency differing from the ultrasonic frequency by one of the contact resonance frequencies of the cantilever. The nonlinear mixing of the oscillating cantilever and the ultrasonic wave at the sample surface generates difference-frequency oscillations at the cantilever contact resonance. The resonance-enhanced difference-frequency signals are used to create amplitude and phase-generated images of nanoscale near-surface and subsurface features. RDF-AFUM phase images of LaRC-CP2 polyimide polymer containing embedded nanostructures are presented. A RDF-AFUM micrograph of a 12.7 μm thick film of LaRC-CP2 containing a monolayer of gold nanoparticles embedded 7 μm below the specimen surface reveals the occurrence of contiguous amorphous and crystalline phases within the bulk of the polymer and a preferential growth of the crystalline phase in the vicinity of the gold nanoparticles. A RDF-AFUM micrograph of LaRC-CP2 film containing randomly dispersed carbon nanotubes reveals the growth of an interphase region at certain nanotube-polymer interfaces.

I. INTRODUCTION

The manufacturing of nanocomposites produced by the embedding of nanostructural constituents into matrix materials has placed increased demands on the development of new measurement methods and techniques to assess the microstructure-physical property relationships of such materials. Although a number of techniques are available for near-surface characterization, methods to assess deeper (subsurface) features at the nanoscale remain largely in development. Cuberes *et al.*[1] and Shekhawat and Dravid[2] have developed methodologies that utilize difference frequencies generated at the surface of a specimen by the interaction of ultrasonic waves incident from below the surface and high frequency oscillations of the AFM cantilever. In both cases the ultrasonic and cantilever driving frequencies are set to generate a difference-frequency signal that is well below the lowest resonant vibrational frequency of the cantilever. The method of Shekhawat and Dravid[2] requires modification to the AFM to implement and they explain that their difference-frequency signal results from a simple linear beating of interacting sinusoidal signals. We introduce a modification of the approaches of Cuberes

et al. and Shekhawat and Dravid that makes direct use of contact resonances of the AFM cantilever to enhance the signal output. A description of the present technique, called resonant difference-frequency atomic force ultrasonic microscopy (RDF-AFUM), is given, together with a brief mathematical analysis of the image generation and contrast. We also present micrographs and analyses that demonstrate the near-surface and subsurface imaging capabilities of the RDF-AFUM technique.

II. RESONANT DIFFERENCE-FREQUENCY ATOMIC FORCE ULTRASONIC MICROSCOPY

Resonant difference-frequency atomic force ultrasonic microscopy (RDF-AFUM) employs an ultrasonic wave launched from the bottom of a sample, while the cantilever of an atomic force microscope engages the sample top surface. The cantilever is driven into oscillation at a frequency differing from the ultrasonic frequency by one of the contact resonance frequencies of the cantilever. The nonlinear mixing of the oscillating cantilever and the ultrasonic wave in the region defined by the cantilever tip-sample surface interaction force generates difference-frequency oscillations at the cantilever contact (linear or nonlinear) resonance. Variations in the amplitude and phase of the bulk wave due to the presence of subsurface nano/microstructures as well as variations in near-surface material parameters affect the amplitude and phase of the difference-frequency signal. These variations are used to create spatial mappings generated by subsurface and near-surface structures.

A schematic of the RDF-AFUM equipment arrangement is shown in Fig.1. A Veeco Instruments Nanoscope IV MultiMode AFM is used for control and processing of the images. The commercial AFM cantilever used in the present work is measured to have a flexural stiffness modulus of 14 N m^{-1} and a fundamental resonance of 302 kHz. An HP model 3325A function generator is used to deliver a 1.8 MHz sinusoidal driving signal to a narrow-band PZT transducer bonded to the surface of the sample opposite the cantilever. A drive signal is sent to the cantilever, operating in intermittent soft contact mode, from the AFM control box to a broad-band piezo-stack under the cantilever. The cantilever drive frequency, amplitude, and the cantilever tip-sample surface separation are varied until the difference between the ultrasonic wave and cantilever drive frequencies correspond to a contact resonance of the cantilever. In the present experiment a cantilever drive frequency of 2.1 MHz, together with the 1.8 MHz ultrasonic drive frequency, generates a difference-frequency signal of approximately 0.3 MHz, corresponding to the lowest contact resonance of the cantilever.

The cantilever drive and transducer drive signals are split and fed to a mixer. The mixer output signal, consisting of sum and difference frequency signals, is sent to the reference input of a PAR model 5302 lock-in amplifier that, because of its limited bandpass, filters out the sum frequency. The AFM photodiode signal, derived from the cantilever response from all sources, is then sent to the signal input of the lock-in amplifier where all frequencies except the difference-frequency are filtered out. The lock-in amplifier measures both the amplitude and phase of the input difference-frequency signal. The appropriate output signal from the lock-in amplifier is fed to the AFM processor to build up either amplitude or phase images as the sample is scanned.

Before commencing a scan, it is useful to determine the set-point value of the feedback parameter that maximizes the amplitude of the difference-frequency signal. The intermittent soft contact mode may be operated while holding one of three parameters constant in the AFM feedback loop: (1) the quiescent deflection of the cantilever, (2) the amplitude of the cantilever's response to the piezo-drive signal ("normal" amplitude), and (3) the phase lag between the cantilever's response to the piezo-drive signal and the drive signal itself ("normal" phase). Calibration curves are taken in which the values of each of these possible feedback parameters are plotted together with the difference-frequency amplitude as a function of the cantilever tip-sample surface separation. From these curves a feedback parameter and a set-point value are chosen to coincide with the maximum difference-frequency signal. Generally, the "normal" amplitude produces the most stable difference-frequency signal when used as the feedback parameter.

As the cantilever tip engages the sample surface, it encounters an interaction force that varies nonlinearly with the tip-surface separation distance. The deflection of the cantilever obtained in calibration plots is related to this force. For small slopes of the deflection versus separation distance, the interaction force and cantilever deflection curves are approximately related via a constant of proportionality. The maximum difference-frequency signal amplitude occurs when the quiescent deflection of the cantilever approaches the bottom of the force well, where the maximum change in the slope of the force versus separation curve (hence maximum interaction force nonlinearity) occurs.

III. RDF-AFUM SIGNAL GENERATION AND CONTRAST

The above description of RDF-AFUM indicates that the difference-frequency signal results from the nonlinear interaction force between the oscillating cantilever tip and the sample surface vibrating in response to incident ultrasonic bulk waves generated at the bottom of the sample. Image contrast is dominated by two principal contributions to the difference-frequency signal: (1) the variations in the amplitude and phase of the ultrasonic wave resulting from features within the sample bulk and (2) the effects of variations in the sample surface contact stiffness on the nonlinear cantilever tip-sample surface interactions. We shall focus on these two contributions to the phase variation of the RDF-AFUM output signal as the cantilever tip scans the sample surface. Since a detailed analytical model of the phase contributions has been reported previously[3], we shall present here only the important results of the model.

The contribution to the variation in phase of the RDF-AFUM output signal from the ultrasonic wave propagating through the bulk of the specimen is obtained by considering a specimen of thickness a/2 having phase velocity c that contains embedded material of thickness d/2 having phase velocity c_d. The embedded material gives rise to a phase variation $\Delta\chi$ in the output signal as the cantilever scans the surface given by[3]

$$\Delta\chi \approx -kd\frac{c}{c_d}\frac{\Delta E}{E}\left[\frac{1}{2}+\frac{e^{\alpha a}\cos ka-1}{(e^{\alpha a}-\cos ka)^2+\sin^2 ka}\right] \qquad (1)$$

where E is the Young modulus of the sample, ΔE is the variation in the Young modulus due to the embedded material, k (= $2\pi/\lambda$, λ = wavelength) is the ultrasonic wave number, and α is the ultrasonic attenuation in the specimen.

The contribution to the phase variations of the RDF-AFUM output signal resulting from variations Δk_s in the sample surface contact stiffness k_s is given by[3]

$$\Delta\Omega_{tot} = (\Delta\beta_{cs} + \Delta\alpha_{cc} + \Delta\phi_{cc} - \Delta\phi_{ss} - \Delta\phi_{cs}) \tag{2}$$

where

$$\Delta\beta_{cs} = \left(\frac{d\beta'_{cs}}{d(\Delta k_s)}\right)_0 \Delta k_s = -\left(\frac{\gamma_s \Delta\omega}{[k_s + F'(z_0)]^2 + \gamma_s^2(\Delta\omega)^2}\right)\Delta k_s \ ; \tag{3}$$

$$\Delta\alpha_{cc} = \frac{\gamma_s \omega_c}{[k_s + F'(z_0)]^2 + \gamma_s^2\omega_c^2}\Delta k_s \quad ; \tag{4}$$

$$\Delta\phi_{cc} = -\frac{A_{cc}}{B_{cc}}\Delta k_s \tag{5}$$

where

$$\begin{aligned} A_{cc} = {} & [\gamma_s k_{cq}^2 + 2F'(z_0)\gamma_s k_{cq} + F'(z_0)^2(\gamma_c + \gamma_s)]\omega_c \\ & + [\gamma_c^2\gamma_s - 2\gamma_s m_c(k_{cq} + F'(z_0))]\omega_c^3 + m_c^2\gamma_s\omega_c^5 \end{aligned} \tag{6}$$

and

$$\begin{aligned} B_{cc} = {} & \{[\gamma_c k_s + \gamma_s k_{cq} + F'(z_0)(\gamma_c + \gamma_s)]\omega_c - \gamma_s m_c\omega_c^3\}^2 \\ & + \{[k_{cq} - m_c\omega_c^2 + F'(z_0)]k_s + F'(z_0)(k_{cq} - m_c\omega_c^2) - \gamma_c\gamma_s\omega_c^2\}^2 \ ; \end{aligned} \tag{7}$$

$$\Delta\phi_{ss} = -\frac{A_{ss}}{B_{ss}}\Delta k_s \tag{8}$$

where

$$\begin{aligned} A_{ss} = {} & [\gamma_s k_{cr}^2 + 2F'(z_0)\gamma_s k_{cr} + F'(z_0)^2(\gamma_c + \gamma_s)]\omega_s \\ & + [\gamma_c^2\gamma_s - 2\gamma_s m_c(k_{cr} + F'(z_0))]\omega_s^3 + m_c^2\gamma_s\omega_s^5 \end{aligned} \tag{9}$$

and

$$\begin{aligned} B_{ss} = {} & \{[\gamma_c k_s + \gamma_s k_{cr} + F'(z_0)(\gamma_c + \gamma_s)]\omega_s - \gamma_s m_c\omega_s^3\}^2 \\ & + \{[k_{cr} - m_c\omega_s^2 + F'(z_0)]k_s + F'(z_0)(k_{cr} - m_c\omega_s^2) - \gamma_c\gamma_s\omega_s^2\}^2 \ ; \end{aligned} \tag{10}$$

and

$$\Delta\phi_{cs} = -\frac{A_{cs}}{B_{cs}}\Delta k_s \tag{11}$$

where

$$\begin{aligned} A_{cs} = {} & [\gamma_s k_{cp}^2 + 2F'(z_0)\gamma_s k_{cp} + F'(z_0)^2(\gamma_c + \gamma_s)](\Delta\omega) \\ & + [\gamma_c^2\gamma_s - 2\gamma_s m_c(k_{cp} + F'(z_0))](\Delta\omega)^3 + m_c^2\gamma_s(\Delta\omega)^5 \end{aligned} \tag{12}$$

and

$$B_{cs} = \{[\gamma_c k_s + \gamma_s k_{cp} + F'(z_0)(\gamma_c + \gamma_s)](\Delta\omega) - \gamma_s m_c(\Delta\omega)^3\}^2 \qquad (13)$$
$$+ \{[k_{cp} - m_c(\Delta\omega)^2 + F'(z_0)]k_s + F'(z_0)[k_{cp} - m_c(\Delta\omega)^2] - \gamma_c\gamma_s(\Delta\omega)^2\}^2 \ .$$

In the above equations the difference frequency $\Delta\omega = (\omega_c - \omega_s)$, ω_c is the cantilever frequency, ω_s is the ultrasonic frequency, γ_s is the sample damping coefficient, γ_c is the cantilever damping coefficient, k_{cq} and k_{cr} are the cantilever stiffness constants corresponding to the q^{th} and r^{th} non-contact resonance modes of the cantilever having frequencies nearest ω_c and ω_s, and $F'(z_0)$ is the effective stiffness constant of the nonlinear interaction force at the cantilever tip-sample surface separation distance z_0.

We obtain from Hertzian contact theory that for isotropic samples the variation in the contact stiffness Δk_s is related to the variation of the Young modulus ΔE of the sample as[4]

$$\Delta k_s = \frac{2r_c(1-\upsilon^2)}{E^2}\left(\frac{1-\upsilon_T^2}{E_T} + \frac{1-\upsilon^2}{E}\right)^{-2}\Delta E \qquad (14)$$

where E_T is the Young modulus of the cantilever tip, υ and υ_T are the Poisson ratios of the sample and cantilever tip, respectively, and r_c is the cantilever tip-sample surface contact radius. It is important to emphasize that the variation ΔE resulting from embedded bulk material is not necessarily equal to that at the specimen surface.

IV. APPLICATION TO NANOCOMPOSITES

We consider here the application of RDF-AFUM to an assessment of the nanostructural features of two nanocomposites having LaRC-CP2 polyimide as the matrix material. One specimen contains a monolayer of gold nanoparticles. The second specimen contains randomly dispersed carbon nanotubes embedded in the matrix.

The Au-polyimide specimen consists of a film of LaRC-CP2 polyimide polymer roughly 12.7 μm thick containing a monolayer of randomly distributed gold particles, roughly 10-15 nm in diameter and embedded roughly 7 μm beneath the specimen surface. The RDF-AFUM micrograph of the nanocomposite is shown in Fig. 2. Fig. 2a is a schematic of the specimen vertical cross-section. The RDF-AFUM phase image is shown in Fig. 2b. The RDF-AFUM image reveals contiguous bright and dark regions over the scan area corresponding to regions of larger (darker regions) and smaller (brighter regions) values of the Young modulus. The maximum variation in phase shown in Fig.2b is approximately 13.2 degrees. The values of the relevant material and cantilever parameters are k_s = 26 N m^{-1}, k_{c1} = 14 N m^{-1}, γ_s = 1,9 x 10^{-6} kg s^{-1}, m_c = 3.9 x 10^{-12} kg, E = 2.4 GPa, a/2 = 12.7 μm, α = 85 m^{-1}, $F'(z_0)$ = - 0.5 N m^{-1}, $\omega_c/2\pi$ = 2.1 MHz, $\omega_s/2\pi$ = 1.8 MHz, and $\Delta\omega/2\pi$ = 0.3 MHz. We calculate from the equations given in Section III that a measured phase variation of 13.2 degrees from the RDF-

AFUM phase image gives a value of approximately 27 percent for the variation in the Young modulus for the material. This value is in good agreement with values in the range 21-29 percent obtained from independent mechanical stretching experiments of pure polymer sheets in which the increase in the modulus is attributed to the growth, during stretching, of a crystalline phase having a larger Young modulus than that of the original amorphous phase[5,6].

The circular feature at the center of the micrograph in Fig.2b (bracketed by two arrows) is thought to be a gold particle surrounded by a slightly larger circular region of material that appears darker in the image than the matrix material in which it is immersed. Equation 1 reveals that the contrast from the particle and its immediate environment is too small to account for the large contrast shown in the micrograph, unless the presence of the gold particle engenders a directional growth during the curing process of crystalline material toward the sample surface. If so, this would create a cylinder of mesophase material containing the gold particle that intersects the sample surface. The dark image-field of the mesophase region indicates that its elastic modulus is larger than that of the matrix material.

The carbon nanotube-polymer specimen consists of a film of LaRC-CP2 polyimide polymer containing bundles of single-walled carbon nanotubes distributed randomly through the bulk of the matrix material. A conventional AFM topographical image of the nanocomposite is shown in Fig.3a. The RDF-AFUM phase image, taken over the same scan area as that of Fig.3a, is shown in Fig. 3b. Comparison of the two images clearly reveals the appearance of subsurface carbon nanotubes in the RDF-AFUM image that do not appear in the AFM topographical scan. Dramatic variations from dark to light to slightly dark contrast occur along the normal to some portions of the boundary between the nanotubes and the matrix material. The variations follow the contour of the nanotubes and suggest the occurrence of an interphase region at the nanotube-polymer interface. The suspected region is lighter than that of either the nanotube or matrix material that bounds it– an indication that the elastic moduli of that region are smaller than that of the matrix material.

V. CONCLUSION

We have presented a scanning probe microscopy technique, resonant difference-frequency atomic force ultrasonic microscopy (RDF-AFUM), that employs the nonlinear mixing of signals from an ultrasonic wave and an oscillating cantilever of an atomic force microscope. The ultrasonic wave is launched from the bottom of a sample and the oscillating cantilever is engaged on the sample top surface. The nonlinear mixing of the oscillating cantilever and the ultrasonic wave in the region defined by the cantilever tip-sample surface interaction force generates difference-frequency oscillations at the cantilever contact resonance. The difference-frequency oscillations are used to create amplitude- and phase-generated images of nanoscale near-surface and subsurface features. We have shown that RDF-AFUM can be used not only to obtain images of such features but when used with the analytical model presented above can also be used to obtain quantitative information regarding the elastic constants of such features. The technique requires only the addition of off-the-shelf instrumentation for implementation and takes advantage of ultrasonic-range probing signals propagating through the bulk of the sample.

REFERENCES

1. M. T. Cuberes, H. E. Alexander, G. A. D. Briggs, and O. V. Kolosov, J. Phys. D: Appl. Phys. **33**, 2347 (2000).
2. G. S. Shekhawat and V. P. Dravid, Science **310**, 89 (2005).
3. S.A. Cantrell, J. H. Cantrell, and P. T. Lillehei, J. Appl. Phys. **101**, 114324 (2007).
4. G. G. Yaralioglu, F. L. Degertekin, K. B. Crozier, and C. F. Quate, J. Appl. Phys. **87**, 7491 (2000).
5. C. C. Fay, D. M. Stoakley, and A. K. St. Clair, High Performance Polymers **11**, 145 (1999).
6. C. Park, Z. Ounaies, K. A. Watson, R. E. Crooks, J. Smith, Jr., S. E. Lowther, J. W. Connell, E. J. Siochi, J. S. Harrison, and T. L. St. Clair, Chem. Phys. Lett. **364**, 303 (2002).

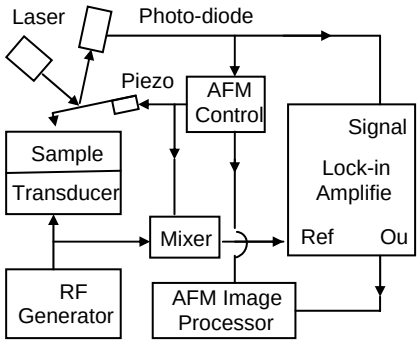

Fig. 1. Schematic of equipment arrangement for the resonant difference-frequency atomic force ultrasonic microscope (RDF-AFUM).

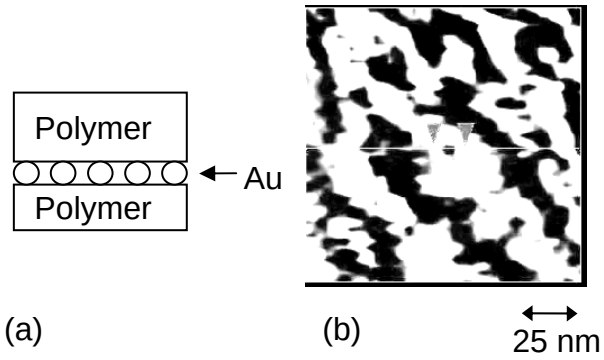

Fig. 2. Results obtained from 12.7 μm thick sample of LaRC-CP2 containing a monolayer of gold particles (10-15 nm in diameter) 7 μm beneath the sample surface: (a) Depiction of specimen vertical cross-section; (b) RDF-AFUM phase image of sample.

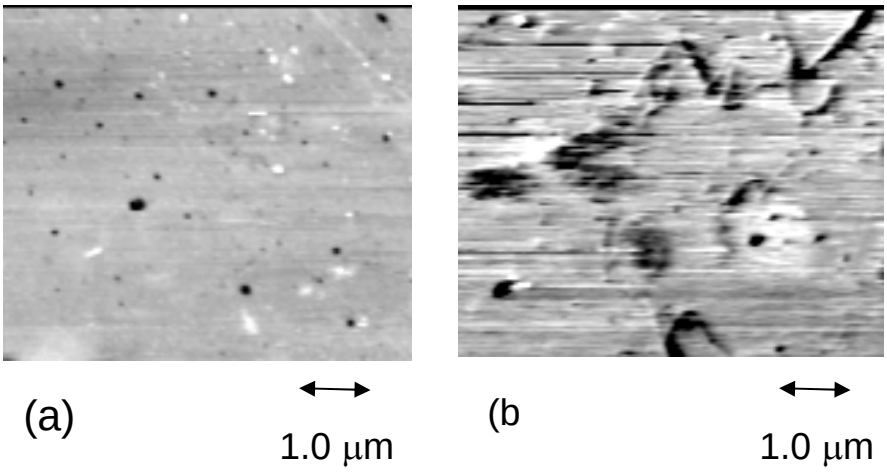

Fig. 3. Results obtained from film of LaRC-CP2 containing randomly dispersed carbon nanotubes: (a) Conventional AFM image; (b) RDF-AFUM phase image of same area of sample as in (a).